

NRC Publications Archive Archives des publications du CNRC

The environments around W Serpentis systems: independent limits on system masses and extended envelopes

Davidge, T. J.

This publication could be one of several versions: author's original, accepted manuscript or the publisher's version. / La version de cette publication peut être l'une des suivantes : la version prépublication de l'auteur, la version acceptée du manuscrit ou la version de l'éditeur.

For the publisher's version, please access the DOI link below. / Pour consulter la version de l'éditeur, utilisez le lien DOI ci-dessous.

Publisher's version / Version de l'éditeur:

<https://doi.org/10.3847/1538-3881/acc580>

The Astronomical Journal, 165, 5, pp. 1-18, 2023-04-04

NRC Publications Archive Record / Notice des Archives des publications du CNRC :

<https://nrc-publications.canada.ca/eng/view/object/?id=4f3c0462-fbe4-42ba-a6dc-35afde29fbc2>

<https://publications-cnrc.canada.ca/fra/voir/objet/?id=4f3c0462-fbe4-42ba-a6dc-35afde29fbc2>

Access and use of this website and the material on it are subject to the Terms and Conditions set forth at

<https://nrc-publications.canada.ca/eng/copyright>

READ THESE TERMS AND CONDITIONS CAREFULLY BEFORE USING THIS WEBSITE.

L'accès à ce site Web et l'utilisation de son contenu sont assujettis aux conditions présentées dans le site

<https://publications-cnrc.canada.ca/fra/droits>

LISEZ CES CONDITIONS ATTENTIVEMENT AVANT D'UTILISER CE SITE WEB.

Questions? Contact the NRC Publications Archive team at

PublicationsArchive-ArchivesPublications@nrc-cnrc.gc.ca. If you wish to email the authors directly, please see the first page of the publication for their contact information.

Vous avez des questions? Nous pouvons vous aider. Pour communiquer directement avec un auteur, consultez la première page de la revue dans laquelle son article a été publié afin de trouver ses coordonnées. Si vous n'arrivez pas à les repérer, communiquez avec nous à PublicationsArchive-ArchivesPublications@nrc-cnrc.gc.ca.



The Environments around W Serpentis Systems: Independent Limits on System Masses and Extended Envelopes

T. J. Davidge

Dominion Astrophysical Observatory, Herzberg Astronomy & Astrophysics Research Center, National Research Council of Canada, 5071 West Saanich Road, Victoria, BC, V9E 2E7, Canada; tim.davidge@nrc.ca, tdavidge1450@gmail.com

Received 2023 January 20; revised 2023 March 16; accepted 2023 March 17; published 2023 April 4

Abstract

Information extracted from the Gaia Data Release 3 is used to examine the stellar contents within projected separations of 10 pc from eight close binary systems that are either classical W Serpentis systems or related objects. The goal is to search for remnant star clusters or moving groups with proper motions that are similar to those of the binaries. While some of the binary systems have proper motions that are distinct from those of the majority of stars within the search area, there is a tendency for W Ser stars to be accompanied by companions with separations on parsec or larger scales. At least three candidate companions are identified within the search area for each system, although in the majority of cases the numbers are much higher. Evidence is presented that SX Cas is near the center of a diffuse cluster. Color–magnitude diagrams of the groupings associated with the binaries are compared with isochrones, and the majority of the groupings are found to have ages ≥ 1 Gyr, indicating that they have an intermediate age. The masses of stars at the main-sequence turnoff of the groupings are estimated, and these provide insights into the initial mass of the donor star in each binary system. Images from the WISE All-Sky Survey are also used to search for circumsystem envelopes. Extended thermal emission is found around six systems in W2 (i.e., $\sim 4.5 \mu\text{m}$) images.

Unified Astronomy Thesaurus concepts: [Interacting binary stars \(801\)](#)

1. Introduction

Plavec & Koch (1978) identified a group of close binary systems (CBSs) that have prominent emission features in the UV. In addition to excess levels of UV emission, these systems exhibit other observational peculiarities, including differences between light-curve maxima (e.g., Davidge & Milone 1984), and circumsystem envelopes (Deschamps et al. 2015). The prototype system is W Serpentis, and a number of other candidate systems have been identified (e.g., Wilson et al. 1984).

The observational evidence suggests that W Ser systems are experiencing rapid mass transfer that occurs after the initially more massive star has evolved to fill its Roche lobe. The period of a system will decrease during the earliest stages of mass transfer, causing elevated mass-flow rates until well after the mass ratio is reversed. In many cases, the final result of the first episode of such rapid mass transfer will likely be a classical Algol configuration. Modeling of systems in which mass transfer is initiated prior to evolution off of the main sequence suggests that the initial rate of mass transfer may be roughly an order of magnitude higher than that in Algol systems (e.g., Nelson & Eggleton 2001). W Ser systems are thus of great importance for understanding the evolution of CBSs in general, and Algols in particular.

The initial masses and ages of the stars in a binary system are of fundamental importance for understanding the relationship between their initial and final states. The moderately long orbital periods of W Ser systems are consistent with the donor star having evolved off of the main sequence (e.g., Van

Rensbergen et al. 2011), and so they are likely undergoing Case B mass exchange. Indeed, the spectral types of the mass-losing stars in W Ser systems are consistent with a giant or supergiant luminosity class and suggest initial masses that are well in excess of solar. Still, caution must be exercised when drawing even broad conclusions about initial masses and evolutionary state, as mixing due to rotation and tidal effects will play a role in defining evolution within CBSs. These processes will prolong the evolution of a star when compared with its static, isolated counterpart, while also potentially altering the chemical content of its outer atmosphere (e.g., Maeder & Meynet 2000; Song et al. 2013). The result of rotation and tidal mixing will make a star appear more luminous than a single nonrotating star of the same mass. Models of evolution in CBSs demonstrate that the evolution of the initially more massive star departs substantially from that expected for an isolated star of the same mass (e.g., Van Rensbergen et al. 2011).

The masses of the component stars in W Ser systems are not known with certainty, as the spectrum of the star that is gaining mass tends to be difficult to detect. These uncertainties are demonstrated in Table 1 of Davidge (2022a), which shows the sizable range in component masses that have been suggested for V367 Cyg. The uncertainty in the component properties of W Ser systems in general is due in part to the evolved nature of the donor star and its brightness when compared with that from the less evolved receiving star. Large-scale mass transfer also forms an accretion disk and other light emitting features that will contribute spectrophotometric features that do not track the orbital motions of the stars, while also masking light from the receiving star. A circumsystem shell may also form, which complicates efforts to identify spectroscopic features from either star. These factors conspire to make W Ser systems single-line spectroscopic binaries.



Original content from this work may be used under the terms of the [Creative Commons Attribution 4.0 licence](#). Any further distribution of this work must maintain attribution to the author(s) and the title of the work, journal citation and DOI.

Table 1
System Properties

Name	R.A. (2000)	Decl. (2000)	π^a (mas)	μ_α^b (mas yr ⁻¹)	μ_δ^b (mas yr ⁻¹)	G (mag)	Source
W Ser	18:09:51	-15:33:00	1.134	0.59	3.06	8.74	Plavec & Koch (1978)
RX Cas	03:07:56	67:34:39	1.818	-3.11	-2.11	8.42	Plavec & Koch (1978)
SX Cas	00:10:42	54:33:29	1.256	-0.82	-2.36	8.75	Plavec & Koch (1978)
W Cru	12:11:39	-58:47:01	0.476	-6.23	0.18	8.02	Plavec & Koch (1978)
V367 Cyg	20:48:00	39:17:16	1.054	-3.36	-3.76	6.91	Plavec & Koch (1978)
V1507 Cyg	19:48:42	29:24:08	1.058	1.55	-5.76	6.89	Wilson et al. (1984)
V644 Mon	06:57:09	-10:49:28	0.877	-0.52	-0.17	6.68	Wilson et al. (1984)
V356 Sgr	18:47:52	-20:16:28	1.478	0.52	-4.85	6.90	Wilson et al. (1984)

Notes.^a Parallax.^b Proper motion, with $\alpha = \text{R.A.}$, $\delta = \text{decl.}$

Given the challenges described above, observational limits on the mass and age of the donor star in W Ser systems that are independent of the orbital motions of the components are of obvious interest. One approach is to identify remnant clusters or moving groups that are associated with these systems. It is not unreasonable to expect that companions to at least some W Ser systems might be present: if the donor stars have initial masses of a few times solar, then they will have ages of a few tens to a few hundreds of Myr. Clusters in this age range are present in the solar neighborhood, although they are admittedly the rump of what was a larger cluster population that has since been depleted.

In the current study, astrometric information is used to search for stars that are physically associated with eight CBS systems that are either confirmed W Ser systems or related objects. Parallax and proper motion measurements that are compiled in the Gaia DR3 (Gaia Collaboration et al. 2016, 2022) are used to identify stars with distances that are comparable to those of the W Ser systems and that have similar motions on the sky. Photometric measurements made by Gaia are used to construct color–magnitude diagrams (CMDs) of the systems. Comparisons are then made with model isochrones.

Selected observational properties of the target systems are listed in Table 1. Magnitudes are in the Gaia system (Jordi et al. 2010). The targets are eclipsing binaries or ellipsoidal variables, and the G magnitudes do not account for variations in light levels due to eclipses and/or activity within the system. The targets include all but one of the systems (β Lyrae) discussed by Plavec & Koch (1978). While it is arguably the best-studied W Ser system, β Lryae is saturated in the Gaia observations and so is not considered here. This being said, Bastian (2019) present evidence of a possible cluster associated with β Lyrae. Three systems from the list compiled by Wilson et al. (1984) with properties that indicate that they are W Ser systems or related objects are also included. Many of these systems are the subject of an ongoing spectroscopic monitoring campaign at the Dominion Astrophysical Observatory (e.g., Davidge 2022a).

All of the systems are within $\pm 10^\circ$ of the Galactic plane, and so are in moderately crowded fields. Six of the systems are within 1 kpc of the Sun, and some have previously been associated with clusters or groupings. For example, Halbedel (1989) suggested that V644 Mon may be part of Canis Majoris OB1. W Cru is the most distant system in the sample, and is located in the Scutum–Centaurus spiral arm in close projected proximity to areas of active star formation. However, the

parallax measurements used here indicate that neither V644 Mon nor W Cru are associated with active star-forming regions. A more detailed discussion of possible membership in known clusters and associations is provided in Section 7.

Additional clues into the evolution of the systems can be gleaned from their circumsystem environments. Simulations suggest that dust shells form around systems that are undergoing rapid mass transfer, and models suggest that emission from the shells may be detected in nearby (i.e., within a few hundred parsecs) systems with space-based infrared (IR) observatories that have only a modest aperture (Deschamps et al. 2015). The shells are expected to dissipate after the pace of mass transfer declines (e.g., Nelson & Eggleton 2001; Deschamps et al. 2015), and so studies of spatially extended dust shells have the potential to identify systems that are in the early stages of mass transfer. In the current study, images obtained as part of the WISE All-Sky survey (Wright et al. 2010) are used to examine the environment within a half-arcmin radius of these systems and search for extended envelopes and very red companions that may be missed at the shorter wavelengths sampled by Gaia. Evidence of spatially extended mid-IR (MIR) emission is found around six of the systems.

2. Data Sets*2.1. Gaia*

Gaia DR3 (Gaia Collaboration et al. 2022) provides basic astrometric information that can be used to identify potential members of remnant clusters and moving groups. This database also contains photometric measurements and reddening estimates that can be used to construct CMDs. The photometry is based on aperture measurements, and so source confusion is a potential concern, as the W Ser stars are in fields near the Galactic plane. However, the selection criteria that are applied here to search for companions restrict the sample to moderately bright objects, the photometry of which is less susceptible to contamination than is the case for stars near the photometric faint limit. Evidence to support the robustness of the photometry comes from the CMDs of star clusters constructed from Gaia photometry that are discussed by Babusiaux et al. (2018). These show well-defined sequences that extend to magnitudes that are fainter than those considered here.

2.2. WISE

The WISE All-Sky Survey (Wright et al. 2010) recorded images in four bandpasses that span the 3–27 μm wavelength interval with angular resolutions $\sim 6''$ – $12''$ (~ 3000 – 6000 au at a distance of 1 kpc). The processed results are available online (Wright et al. 2019). Here, we focus on images taken through the W2 ($\lambda_{\text{cen}} = 4.6 \mu\text{m}$) filter. Processed image tiles were downloaded from the IPAC website,¹ and these were used to search for extended circumstellar emission. Evidence for resolved emission around some of the systems is presented in Section 6.

3. Source Selection

Potential companions of the W Ser systems are identified using a combination of the parallaxes, proper motions, and locations on the sky of sources that are compiled in the Gaia DR3. It is anticipated that any companions will belong to diffuse clusters or moving groups. Two samples are generated with this expectation in mind, and the selection criteria for each of these samples are described in the following subsections.

3.1. The Baseline Sample

An initial list of possible companions was made by identifying stars that have projected distances on the sky within ± 10 pc of each system, where the angular extraction radius is calculated using the Gaia DR3 parallax measurement. A 10 pc radius samples an area that is $4\times$ larger than that subtended by the main body of the Hyades. While generous, such a large initial search area was employed because heretofore unidentified old clusters and moving groups are expected to be diffuse.

Stars in the search area were then filtered according to parallax. While this is a seemingly a straightforward process, potential systematic uncertainties in the parallaxes should be considered when selecting a suitable range to search for companions. Lindegren et al. (2021) identify brightness, color, and location on the sky as possible sources of systematic errors in Gaia parallaxes. These uncertainties have been reduced with progressive Gaia data releases (e.g., Ren et al. 2021; Stassun & Torres 2021).

Location on the sky is likely not a concern for the selection of possible companions in the context of systematic uncertainties in the parallaxes. This is because the search is restricted to a comparatively small angular extent (less than a degree in radius) centered on each system. All parallaxes for candidate companions to a W Ser system should then have a similar location-based bias. While such a bias may affect the measurement of absolute quantities, such as distance, absolute magnitude, and age, the selection of a sample of possible companions to the W Ser systems will not be affected.

Systematic uncertainties that are related to the color and brightness of a source are potentially of greater concern, as Lindegren et al. (2021) find that the parallax of sources with the same distance may differ by a few tens of mas depending on their brightness and color. However, there are hints that such biases may not be significant for the sources examined in this study. The faint limit imposed by selection criteria that are described below is in the range $G = 16$ – 18 . Muzic et al. (2019) find no systematic trend in parallax among blue stars in the

young open cluster NGC 2244 down to $G \sim 16$ in Figures 4 and 5 of their paper. As for systematic errors in parallax that might arise due to color, in most cases the final samples of objects found in the current work are dominated by blue stars, reducing the influence of color-related systematics. The CMDs of distant open clusters discussed by Babusiaux et al. (2018) provide further evidence that systematic errors in parallax due to brightness and color may not be a major concern.

Even though there is evidence that systematic errors in brightness and color may be small, we take the cautious approach of applying a wide parallax selection filter. The maximum systematic errors in parallax due to color are comparable to the uncertainties in the parallaxes of the W Ser stars at the 1σ to 2σ levels. To account for possible systematic errors of this size, stars were extracted from the database that had parallaxes within 2σ of the parallax of the W Ser star. This sampled line-of-sight depths ranging from ± 15 pc for RX Cas (the nearest system) to ± 270 pc for W Cru (the furthest system). While fostering contamination from objects that are not related to the W Ser star, this criterion allowed objects that may otherwise be missed due to a systematic error in parallax but could still be possible members of a cluster/moving group to be included. Stars that are not related to the W Ser systems are identified using proper motion measurements (see next section).

The sample was further restricted to sources that have 1σ random uncertainties in parallax that are less than the 2σ random error estimates for the host W Ser systems. Not only does this limit the number of interlopers with uncertain parallaxes, but it also effectively sets the faint limit of the samples to $G \sim 16$ – 17 . This is a relatively benign filter in the context of estimating system ages, as stars with large uncertainties in the parallax tend to be significantly fainter than the main-sequence turnoff (MSTO) in intermediate-age groups at the distances examined here, and so contain little information about age.

Filtering based on angular extent on the sky and distance results in a list of candidate companions that are referred to as the baseline sample. Gaia DR3 lists proper motions in decl. and R.A., and the proper motion diagrams for baseline sample objects are shown in Figures 1(a) and (b). The distribution of points in the proper motion diagram of W Cru in Figure 1(b) is much more compact than for the other systems. This is a distance effect—proper motions will decrease with increasing distance among sources that have a given space velocity.

Evidence for clumping is seen in these panels, and in some cases these concentrations are not centered on the proper motions of the W Ser systems, which are indicated with the dotted lines in these figures. A good example is V1507 Cyg, which is offset from a denser clump of sources on the proper motion diagram. The presence of proper-motion-based groupings that appear to be unrelated to the W Ser stars is perhaps not surprising, given the low Galactic latitudes that are examined.

There is also a tendency for some of the W Ser systems to be offset from the centers of the data distributions in the proper motion diagrams. W Ser and RX Cas are the most obvious examples, with their kinematic properties differing from those of many of their immediate neighbors. These systems are not completely isolated on the proper motion plane, and it is likely that stars that are near them on the proper motion plane share a common kinematic (and hence probably an evolutionary)

¹ <https://irsa.ipac.caltech.edu/applications/wise/>

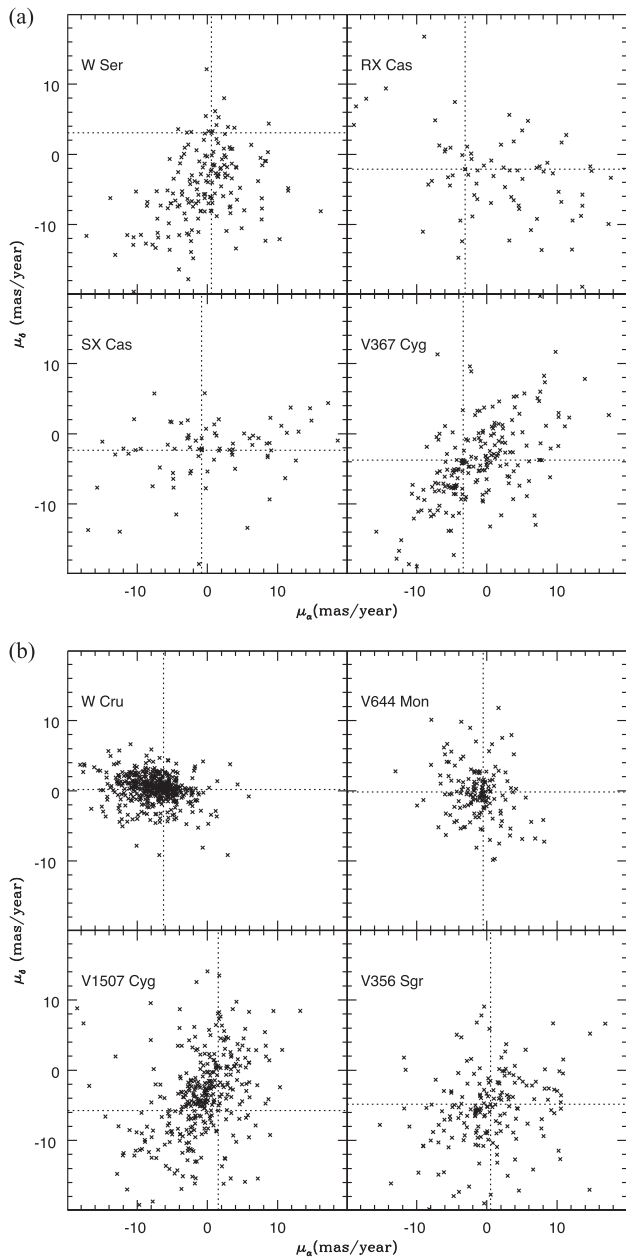


Figure 1. (a) Proper motion diagrams of stars in the baseline samples of W Ser, RX Cas, SX Cas, and V367 Cyg. μ_δ and μ_α are proper motions in decl. and R. A. in mas yr^{-1} . The dotted lines mark the proper motions of the W Ser systems. Typical 1σ random errors in the proper motions of all stars in these diagrams are ± 0.02 – 0.03 mas yr^{-1} along each axis. The vast majority of objects in the baseline samples are scattered throughout the diagrams and are likely not related to the W Ser systems. Still, there are objects that have proper motions that are similar to those of the W Ser systems. The locations of W Ser and RX Cas indicate that their kinematic properties differ in a systematic way from those of most other stars in their baseline samples. (b) Same as Figure 1(a), but showing the proper motion diagrams of baseline sample stars near W Cru, V644 Mon, V1507 Cyg, and V356 Sgr. There are obvious concentrations on the proper motion plane around V644 Mon and W Cru. The large baseline sample for W Cru is due to the substantial line-of-sight distance that is sampled for this system. A concentration of objects is evident in the proper motion plane of V1507 Cyg that is offset from the proper motions of that system.

heritage. The identification of these objects is discussed in the next subsection. Given that the dynamical properties of a star will evolve with time, then one *possible* explanation for the locations of some of the W Ser systems is that they have ages that differ from the majority of their neighbors.

3.2. The Final Sample

Physical proximity is but one consideration for the identification of physically related stellar groupings, especially in the low Galactic latitude fields that are examined here. Additional filtering was done using projected spatial motions, with stars in the baseline sample identified that have proper motions that are similar to those of the W Ser stars. Selection based on proper motion samples only two axes of a three-dimensional spatial motion vector. Nevertheless, while there are radial velocity estimates for some stars, these are not available for the vast majority of stars in the baseline samples, and so radial velocities are not considered.

The apparent lack of grouping around many of the W Ser systems in the proper motion diagrams suggests that, in the majority of cases, any remnant clusters—if present—are not well populated. W Cru and V644 Mon appear to be exceptions, although these are also the most distant systems and so will have the most compact proper motion distributions. Still, given that many of the systems are at similar distances, it is possible to determine if there is at least a general tendency for these systems to be accompanied by companions. To do this, the proper motion diagrams of W Ser, RX Cas, SX Cas, V367 Cyg, and V356 Sgr were combined, and the results are shown in the top panel of Figure 2. To combine the samples, the proper motions of the host systems were subtracted from the proper motions of their baseline samples. The proper motions used to construct Figure 2 are then offsets from that of the host system. V1507 Cyg was excluded due to the concentration of objects in its proper motion diagram to the upper left of the W Ser star in Figure 1(b), as such a collection of stars will skew the comparison in Figure 2.

A concentration of objects is evident near the origin in the top panel of Figure 2, indicating a general tendency for the W Ser stars to have companions that are distributed over spatial scales of many parsecs and are moving with them on the sky. This is quantified in the lower panel of Figure 2, where the density of objects in the proper motion diagram is shown as a function of the offset in mas yr^{-1} from the origin. The number density in the innermost bin does not include the W Ser systems, and the error bars reflect counting statistics.

A uniform distribution of objects on the proper motion plane will produce a flat trend in the the lower panel of Figure 2. Not including the W Ser systems, there is an excess number of objects that have proper motions within 0.5 mas yr^{-1} of the origin. The density in the proper motion plane drops at larger offsets, such that the density gradually decreases with increasing offset out to 4.5 mas yr^{-1} . The modest uptick in the number of sources near the 2 mas yr^{-1} offset is due to the clump of objects to the lower left of the origin in the upper panel of Figure 2, centered near $\Delta\mu_\delta \sim -1 \text{ mas yr}^{-1}$ and $\Delta\mu_\alpha \sim -2 \text{ mas yr}^{-1}$.

Based on the comparisons in Figure 2, potential companions were extracted from the baseline samples by applying a $\pm 1.5 \text{ mas yr}^{-1}$ cut around the proper motion of each W Ser system. This extraction criterion was adopted as a compromise between the desire to sample as many potential companions as possible and the need to maintain some degree of contrast with respect to the background sample. The one exception is W Cru: as this system is roughly twice as far as the other systems, an extraction criterion of $\pm 0.75 \text{ mas yr}^{-1}$ (i.e., one half that applied to the other systems) was applied.

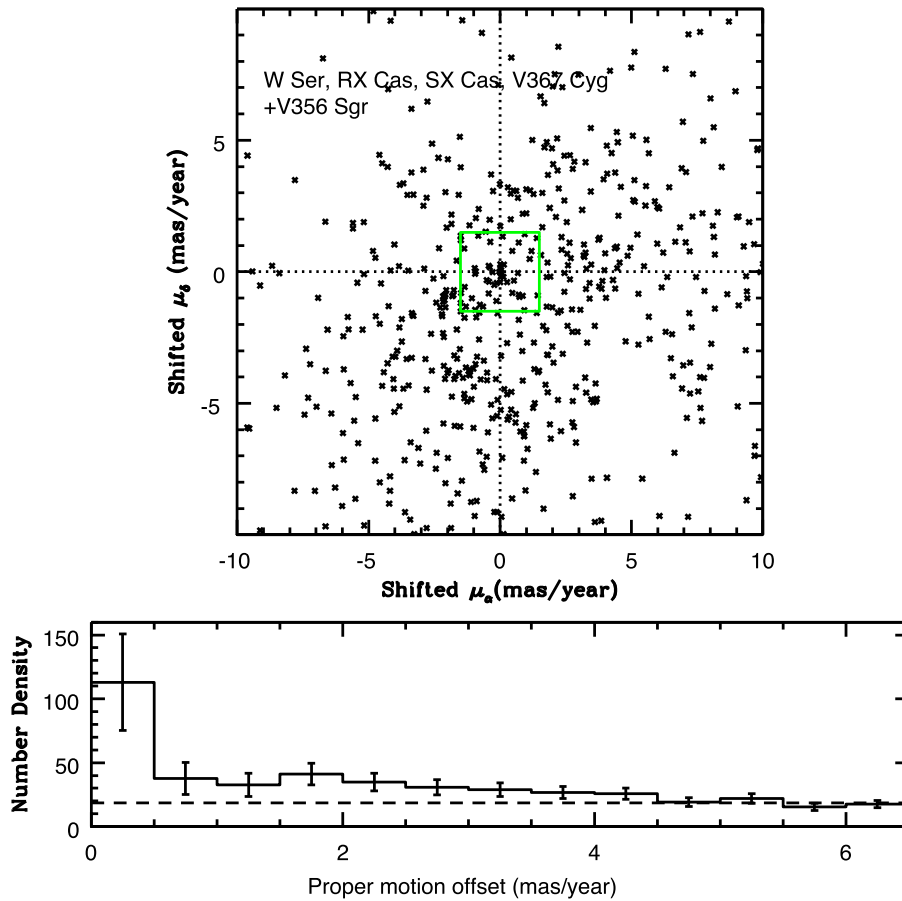


Figure 2. (Top panel) Composite proper motion diagram of the W Ser, RX Cas, SX Cas, V367 Cyg, and V356 Sgr baseline samples. The proper motions of each system have been subtracted from those of individual stars to align the samples. The origin is at the intersection of the dotted lines. There is an apparent concentration of objects at the origin, indicating a general tendency for the W Ser systems to have companions. The green square is 3 mas yr^{-1} on a side, and shows the approximate extraction area adopted to identify companions for these stars. (Bottom panel) Number density of sources in the top panel (i.e., the number of objects per $\text{mas}^2 \text{ yr}^{-2}$) vs. the radial offset from the origin. The dashed line shows the average density in the four bins with the greatest offsets from the origin, where the density in proper motion space appears to be stable. While the error bars are large, there is a tendency for the density of objects in proper motion space to decrease with increasing offset out to $\sim 4.5 \text{ mas yr}^{-1}$.

We emphasize that the companions identified in proper motion space are not physically close to the W Ser systems at the present day. Rather, the spatial distributions of these objects on the sky (see Section 4) indicate that they are distributed over the entire area that is surveyed around the host systems. There is thus no evidence that these objects were once close companions to the W Ser systems and so may have played a direct role in shaping their evolution. Still, the presence of companions suggests that the initial properties of the clusters in which the W Ser systems formed were such that the clusters have not been completely obliterated over $\sim 1 \text{ Gyr}$ timescales.

Objects that are extracted from the baseline samples based on their proper motions form the final samples. The fraction of stars in the baseline sample that makes it into the final sample varies from system to system, although it is apparent from Figures 1(a) and (b) that this fraction is small in most cases. SX Cas and RX Cas have the smallest fraction of baseline sample objects that make it into the final sample, reflecting the small number of objects near the intersections of the dashed lines in Figure 1(a).

4. The Projected Distribution and Photometric Properties of Potential Cluster Members

4.1. On-sky Distribution

The projected location of objects on the sky provides insights into membership in a stellar group. Nevertheless, while

evidence for clustering on the sky is obviously desirable when searching for companions, it is not essential. In fact, given the low Galactic latitudes of these fields, it might be anticipated that diffuse clusters and moving groups will not stand out in a statistical sense when compared with background populations.

The projected distributions of objects in the baseline and final samples are compared in Figures 3(a) and (b). At first glance, the distributions of the two samples appear to differ in some cases. However, what is the statistical significance of such differences? The azimuthal and radial distributions of stars in the baseline and final samples around each system have been examined to answer this question.

The angular distributions of the baseline and final samples are compared in Figure 4. Position angles were measured about each W Ser system, with 0° to the east. Cumulative number counts, which are the total number of objects up to a given angle in 30° wide bins, are shown. The results have been normalized to the number of objects in each sample.

A sample of objects that is uniformly distributed on the sky will form a diagonal sequence in Figure 4, and the dotted lines in each panel mark this trend. The baseline samples for the majority of systems more-or-less follow the trend expected for a uniformly distributed sample, although V367 Cyg and V644 Mon are possible exceptions. There is a tendency in both cases for objects in the baseline sample to concentrate between 180° and 360° , indicating a lopsided distribution on the sky. A KS

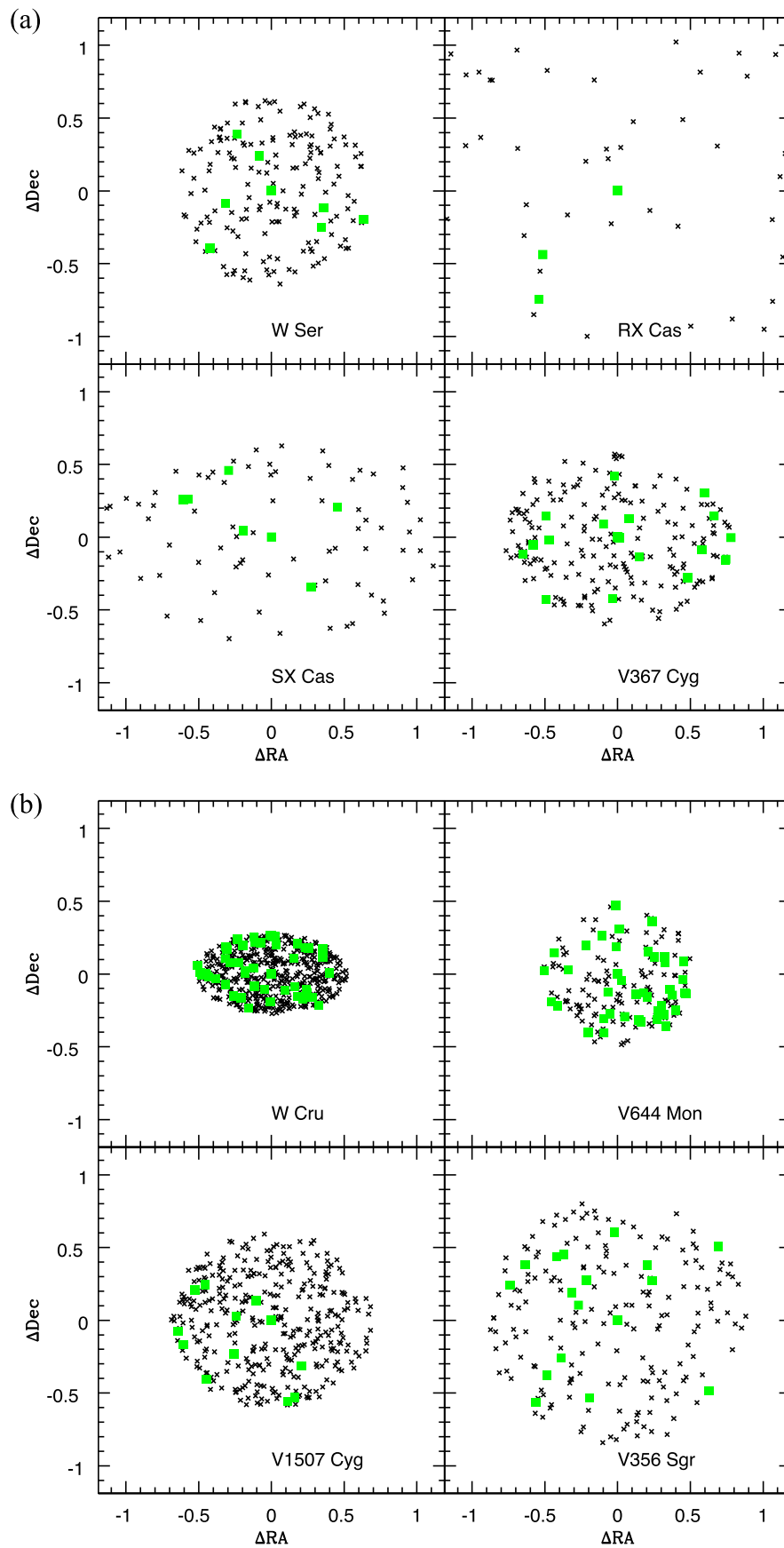


Figure 3. (a) Locations on the sky of stars in the baseline (black crosses) and final (green squares) samples of W Ser, RX Cas, SX Cas, and V367 Cyg. Offsets in R.A. and decl. from each W Ser system are plotted. (b) Same as Figure 3(a), but showing the locations of stars near W Cru, V1507 Cyg, V644 Mon, and V356 Sgr. The large number of objects in the W Cru final sample is a consequence of the large volume sampled around this system.

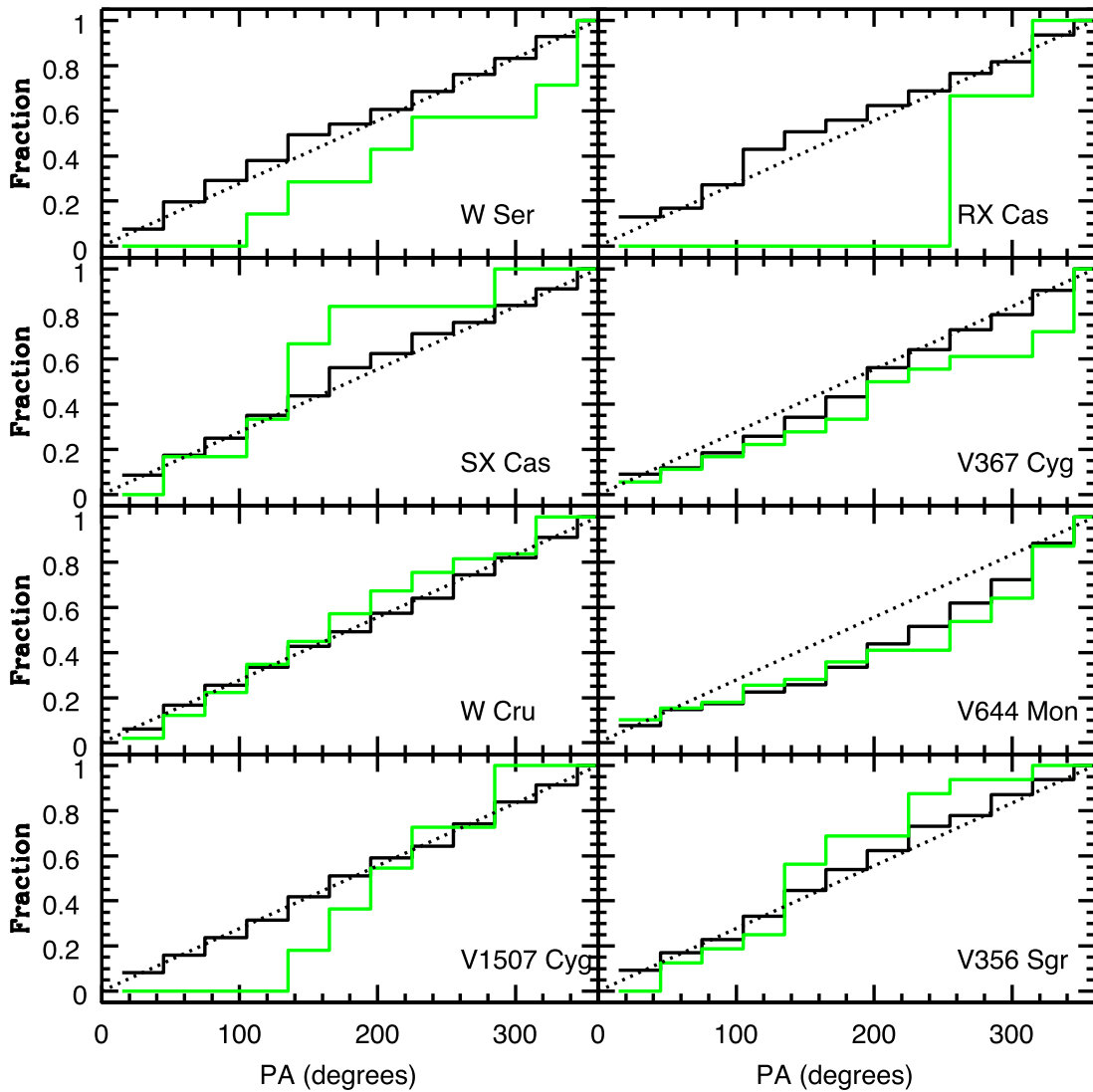


Figure 4. Angular distributions of stars in the baseline (black line) and final (green line) samples. Cumulative number counts in 30° wide bins are shown along the y-axis. Position angles (PAs) were measured centered on the W Ser systems, with 0° to the east. The distributions have been normalized to the total number of objects in each sample. Objects that are uniformly distributed on the sky define a diagonal that is indicated by the dotted lines. In most cases, the baseline samples are consistent with a uniform distribution. Possible exceptions are V367 Cyg and V644 Mon, where there is a tendency for objects to be concentrated between 260° and 360° . A Kolmogorov–Smirnov (KS) test indicates that the angular distributions defined by the baseline and final samples of RX Cas and V1507 Cyg differ at the 75%–85% confidence level.

test confirms that these differences are significant in excess of the 90% confidence level.

V367 Cyg and V644 Mon have locations on the sky that are close to star-forming regions that have high stellar densities. However, the lopsided angular distributions in the baseline samples of these systems are likely not due to nearby young clusters. V367 Cyg is roughly a degree away from the center of the open cluster M29, and the parallaxes of V367 Cyg and M29 differ by an amount that far exceeds the range used to define the baseline sample. As for V644 Mon, the location of that system on the sky coincides with Group 12 identified by Santos-Silva et al. (2021) in their study of CMa OB1. While some of the stars in this group have proper motions that overlap with V644 Mon, the range of parallaxes that are used to extract the V644 Mon baseline sample do not overlap with those of objects in that group (Figure 2 of Santos-Silva et al. 2021). The proper motion diagrams of V367 Cyg and V644 Mon also do not show noticeable concentrations that are offset from the proper motions of the systems, as might be expected if there

was substantial contamination from a kinematically unrelated cluster. In fact, V644 Mon is near the center of the dominant cloud of objects in the proper motion diagram. We suspect that the asymmetric distributions of baseline objects near V367 Cyg and V644 Mon are due to foreground obscuration.

If the baseline samples are dominated by field stars, then a difference between the angular distributions of the baseline and final samples might be expected if the W Ser systems are in fossil groups. For example, a lopsided distribution in the final sample could occur if a W Ser system is embedded in a cluster or moving group but is not near its geometric center. A skewed angular distribution might also occur if the W Ser systems formed in filaments that have not yet dissipated; such a scenario has been suggested for the massive binary V640 Mon (Davidge 2022b).

The position angle distributions of the baseline and final samples in Figure 4 have been compared with the KS statistic. The most statistically significant differences between the angular distributions of these two samples are those for RX

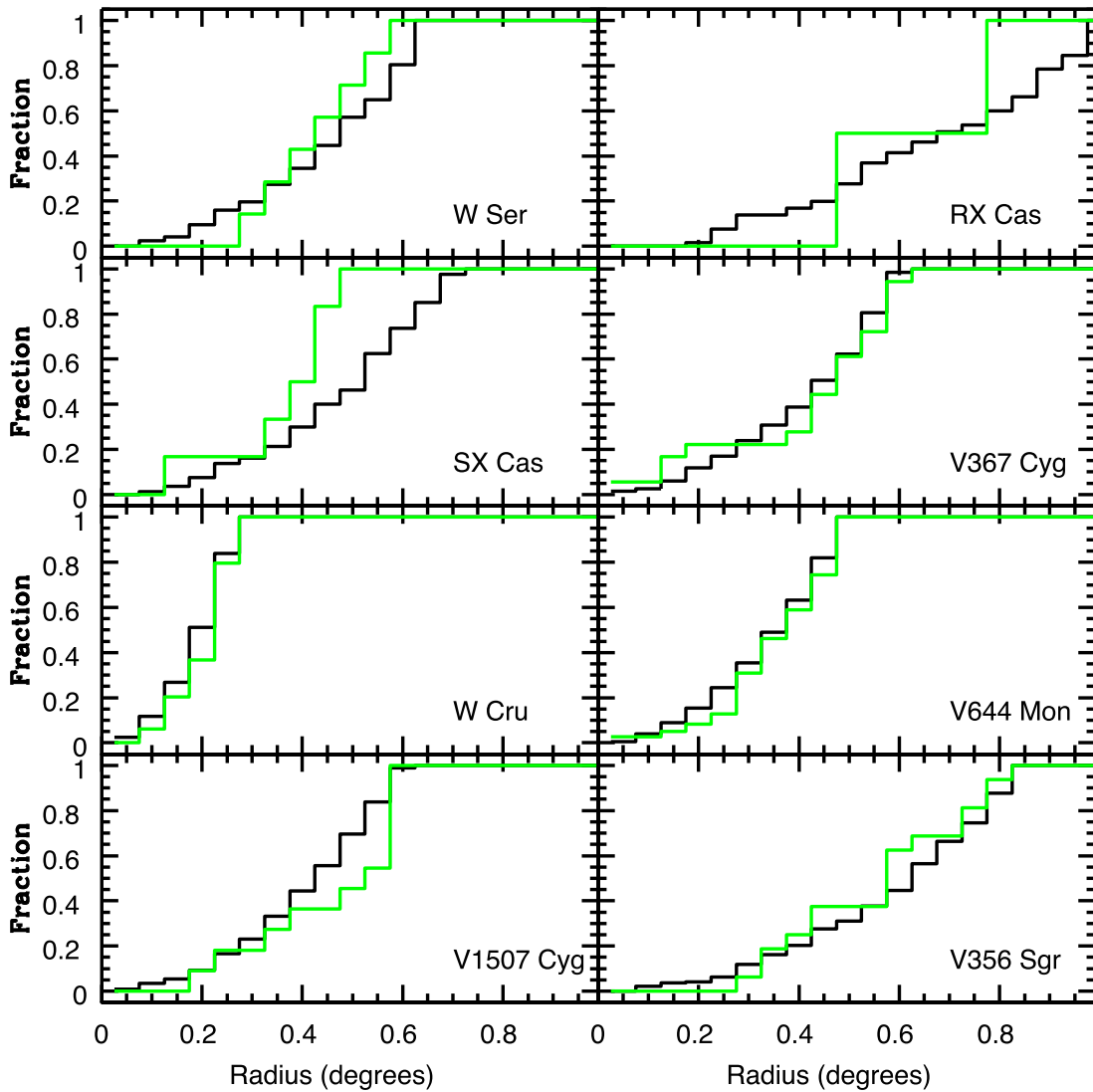


Figure 5. Same as Figure 4, but showing radial distributions centered on the W Ser systems. Cumulative number counts have been measured in $0^{\circ}05$ angular bins on the sky centered on the W Ser systems, with the distributions normalized to the total number of counts in each sample. System-to-system differences in the slopes and total angular extents of the baseline distributions are due to the wide range in system distances. With the exception of SX Cas, and to a lesser extent W Cru and V1507 Cyg, the radial distributions of the baseline and final samples are not significantly different.

Cas (85% confidence) and V1507 Cyg (75% confidence). V1507 Cyg is located on the sky midway between the open clusters NGC 6834 and Turner 9. However, contamination from stars in those clusters does not cause the skew in the NGC 1507 final sample distribution, as both clusters have parallaxes that are far smaller than that of V1507 Cyg (Cantat-Gaudin & Anders 2020) and so do not contribute stars to the baseline and final samples.

The radial distributions of sources centered on the W Ser systems provide another probe of grouping, if it is assumed that the W Ser system is in a cluster and if the baseline stars are an unclustered field component. The radial distributions of the final and baseline samples are compared in Figure 5. As with Figure 4, the panels in Figure 5 show cumulative number counts up to a given angular offset from each W Ser system. A bin width of $0^{\circ}05$ has been adopted. System-to-system differences in the total angular coverage on the sky are due to the range in system distances.

The KS statistic indicates that the baseline and final radial distributions of SX Cas differ at the 95% confidence level. This

difference is in the sense that stars in the final sample of SX Cas have a more compact distribution on the sky than those in the baseline sample. That the angular distributions of the baseline and final samples of SX Cas do not differ suggests that SX Cas is likely close to the center of a structurally distinct stellar ensemble. Weaker evidence for clustering is found for W Cru and V1507 Cyg, where the radial distributions of the final and baseline samples differ at roughly the 70% confidence level.

4.2. CMDs

The CMDs of the baseline and final samples are shown in Figures 6(a) and (b). The faint limits fall between $G \sim 16$ and 17, and these are largely defined by the maximum allowable error in the parallaxes. The primary region of interest in the CMDs when estimating ages is the upper portions of the main sequence, and this is well above the faint limit in all cases. The main sequence in most cases tends to be well defined, as expected given the moderately small dispersion in distance that

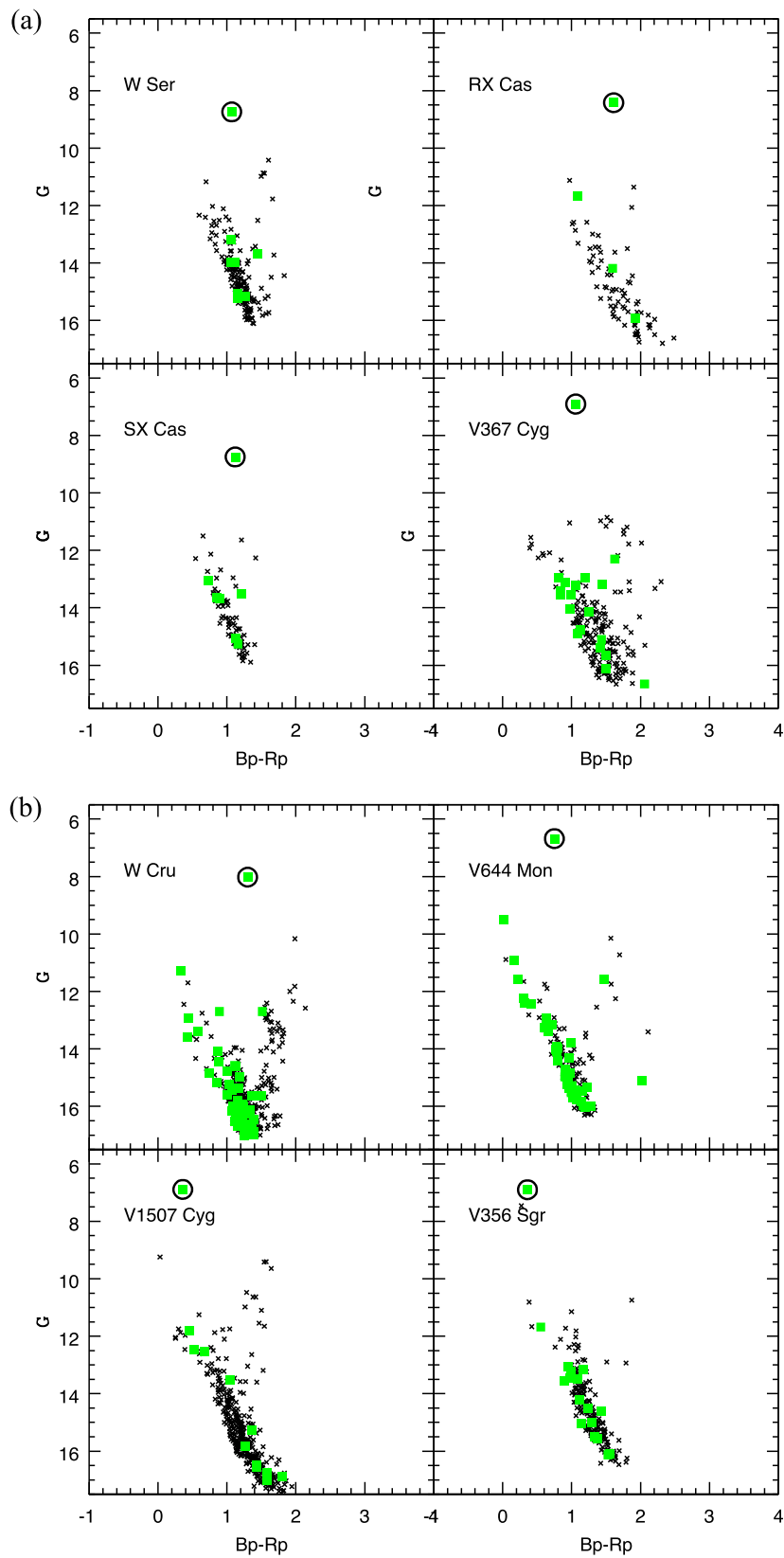


Figure 6. (a) (G , $Bp - Rp$) CMDs of stars in the baseline (black crosses) and final (green squares) samples of W Ser, RX Cas, SX Cas, and V367 Cyg. The W Ser system, which is circled in black in each panel, is the brightest object in each CMD. The main sequence is the dominant feature in each CMD. The stars with red colors that are above and to the right of the main sequence are likely SGB stars that belong to an intermediate-age field population. (b) Same as Figure 6(a), but showing the CMDs for W Cru, V644 Mon, V1507 Cyg, and V356 Sgr. SGB sequences are seen above and to the right of the main sequence in the baseline sample CMDs of W Cru, V644 Mon, and V1507 Cyg.

results from selection based on parallax, coupled with the expectation of solar-like metallicities based on the locations of the target fields at low Galactic latitudes. The main sequences in the baseline sample CMDs of W Ser, SX Cas, V644 Mon, and V356 Sgr have a width along the color axis that is comparable to the dispersion in the CMDs of clusters examined by Babusiaux et al. (2018).

The narrow main sequence notwithstanding, there is evidence that the baseline samples contain stars with a range of ages, as expected if they contain a dominant field component. A red subgiant branch (SGB) with a G brightness that is comparable to, or fainter than, the apparent MSTO of the baseline sample is present in most CMDs. This is a standard feature in disk field CMDs (e.g., Babusiaux et al. 2018), and is due to the presence of stars that have older ages than those near the MSTO. There is also scatter among baseline sample stars in the CMDs near the MSTO. While an age dispersion is one possible explanation, binarity, differences in rotation rates, and differential reddening can also broaden this part of the CMD.

Unlike the baseline samples, the final samples might be expected to consist of a homogeneous ensemble of objects, given that they have been selected with the additional criterion of similar kinematic properties. The brightest main-sequence stars in the final samples of W Ser, SX Cas, and V367 Cyg tend to be fainter than main-sequence objects in the baseline samples, indicating that these systems may not be as young as neighboring stars. This is not a surprising result, given that the systems are at low Galactic latitudes, where a population of young field stars might be expected. In contrast, the brightest blue stars in the final sample CMDs of W Cru, V644 Mon, and V1507 Cyg are at or near the MSTO of the baseline samples associated with those systems.

5. Age and Mass Estimates

5.1. Comparisons with Isochrones

Comparisons have been made with the MESA Isochrones and Stellar Tracks (MIST; Paxton et al. 2011, 2013, 2015; Choi et al. 2016; Dotter 2016). As the W Ser systems are in the Galactic disk within a few kpc of the Sun, a solar metallicity is assumed. The sequences used here assume nonrotating stars (i.e., $\frac{v}{v_{\text{crit}}} = 0$), and adopting models with $\frac{v}{v_{\text{crit}}} = 0.4$ will change the positions of the isochrones by ~ 0.1 mag toward brighter values along the vertical axis for the range of ages found for the stellar groupings. The use of these rotating models will then not have a major impact on age estimates. The Gaia database includes reddenings and selective extinction estimates for the vast majority of stars in the baseline sample, and the isochrones have been shifted to account for interstellar extinction by applying the median A_G and A_{BpRp} values for the stars in the baseline samples.

The CMDs are compared with isochrones in Figures 7(a) and (b). The isochrone placement for each system is based on the parallax measurement of that system with no correction for potential systematic effects due to brightness, color, etc. The isochrones have also been shifted using the median A_G and A_{GpRp} values of objects in the baseline samples that are listed in the Gaia database.

Age estimates are listed under the system names in these figures. These are based on a “by eye” matching of isochrones with the final sample data. These estimates are anchored on the MSTO, and when available, the SGB. With the exceptions of

W Cru and V644 Mon, the CMDs of stars in the final sample are matched with isochrones that have ages $\log(t_{\text{yr}}) \geq 9$. The comparisons with isochrones thus suggest that the classical W Ser systems identified by Plavec & Koch (1978) are intermediate-age objects.

For four of the systems (W Ser, SX Cas, V367 Cyg, and V1507 Cyg), the age estimate is based on a match to both the MSTO and SGB. The final sample CMD of V367 Cyg has a well-defined MSTO region that includes an SGB, and the SGB is matched by the isochrone that is anchored on the brightest main-sequence star. The age estimate for this system is thus considered to be the most secure in our sample.

There are no candidate SGB stars in the final samples of RX Cas, V644 Mon, and V356 Sgr to guide comparisons with the isochrones. W Cru is another system for which the location of the SGB may be problematic: while there are two stars that define an apparent SGB, there is also a blue star in the final sample that is ~ 2 mag above the next-brightest main-sequence star in the CMD. For these four systems, the age estimate immediately under the system name is based on the brightest main-sequence star, while the age in brackets is based on the second-brightest MS star. The second entry for these systems thus assumes that the brightest blue star is a blue straggler or an interloper from the field. In the case of W Cru, the isochrone that uses the second-brightest main-sequence star to define the MSTO is more-or-less consistent with the location of the two candidate SGB stars.

The W Ser systems tend to have absolute G magnitudes that are at least 2 mag brighter than the next-brightest objects in the final samples. Of particular interest is that the absolute magnitudes and colors of W Ser, RX Cas, and SX Cas agree to within a few tenths of a magnitude, and so these systems may share similar intrinsic properties. Evidence to support this notion comes from the brightest main-sequence stars in their final samples. The MSTO brightnesses of W Ser and SX Cas agree to within a few tenths of a magnitude, whereas the brightest blue star in the RX Cas final sample is ~ 1 mag brighter than in the final samples of W Ser and SX Cas. The absolute magnitude of the brightest main-sequence star in RX Cas is not vastly different from that of W Ser and SX Cas, even though there are only three stars in the final sample of that system. To the extent that the three systems have similar intrinsic properties, a comparison of the age estimates for these systems based on the MSTO suggests an uncertainty in the $\log(t_{\text{yr}})$ estimates of ~ 0.1 – 0.2 dex.

Small-number statistics contribute to uncertainties in the location of the MSTO for systems where the final sample is poorly populated. However, the comparison of the MSTO brightness estimates for W Ser, RX Cas, and SX Cas in the previous paragraph suggests that stochastic effects contribute only a 0.1–0.2 dex error in $\log(t_{\text{yr}})$. Contamination from even a single field star that has proper motions that are fortuitously similar to those of the W Ser systems might also bias the age estimates of those systems with only small numbers of stars in the final sample.

A comparison between the isochrones and the baseline CMDs might provide guidance into field star contamination. In most cases, the baseline sequences along the SGB are matched by $\log(t) = 9.5$ isochrones, and this is close to the age estimates for W Ser, RX Cas, SX Cas, V367 Cyg, and V356 Sgr. Even though the age estimate for V367 Cyg is consistent with that of the SGB population in the baseline sample, the CMD of the

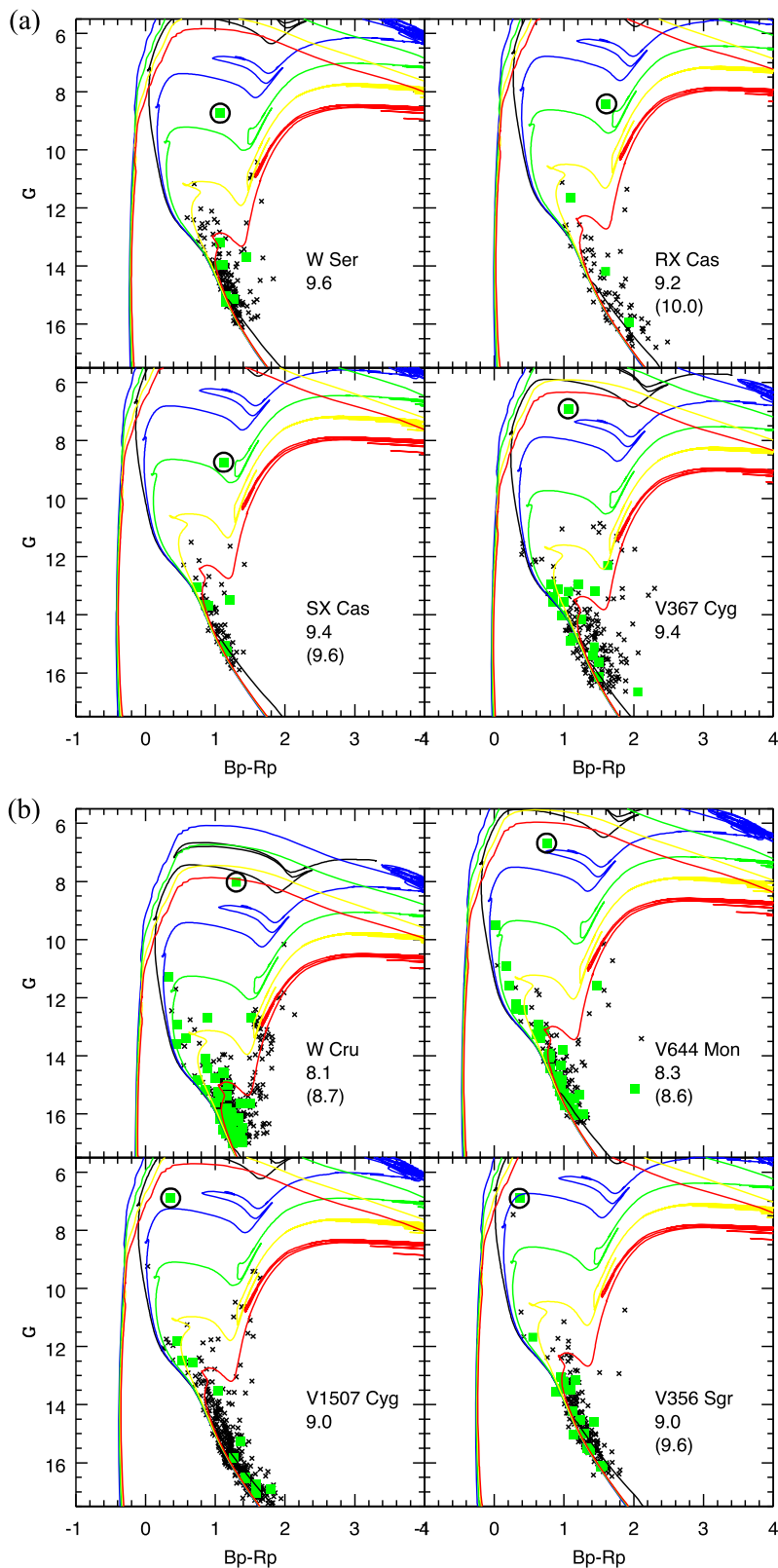


Figure 7. (a) Comparisons with nonrotating, solar-metallicity MIST isochrones. The sequences have ages $\log(t_{\text{yr}}) = 7.5$ (black), 8.0 (blue), 8.5 (green), 9.0 (yellow), and 9.5 (red). Points are plotted using the same identification scheme as in Figure 6(a). The $\log(t_{\text{yr}})$ estimated for each system is shown under the system name. The entries in brackets for RX Cas and SX Cas are age estimates that are based on the second-brightest main-sequence star, as an SGB is not visible in the final-sample CMDs of those systems. The estimated uncertainties in the ages are 0.1–0.2 dex (see text). (b) Same as Figure 7(a), but showing CMDs for W Cru, V644 Mon, V1507 Cyg, and V356 Sgr. Two age estimates are given for W Cru, V644 Mon, and V356 Sgr, and the entry in brackets is that based on the second-brightest main-sequence star.

Table 2
Age and MSTO Masses

Name	$\log(\text{Age})_{0.0}^a$	MSTO $\text{Mass}_{0.0}^b$ (M_{\odot})	Total System $\text{Mass}_{0.0}^c$ (M_{\odot})	M2016 Mass^d (M_{\odot})
W Ser	9.6	$1.1^{+0.2}_{-0.1}$	$2.2^{+0.4}_{-0.2}$	2.5
RX Cas	9.2 (10.0)	$1.5^{+0.3}_{-0.2}$ ($1.0^{+0.1}_{-0.1}$)	$3.0^{+0.6}_{-0.4}$ ($2.0^{+0.2}_{-0.2}$)	7.6 ± 0.6
SX Cas	9.4 (9.6)	$1.3^{+0.2}_{-0.2}$ ($1.1^{+0.2}_{-0.1}$)	$2.6^{+0.4}_{-0.4}$ ($2.2^{+0.4}_{-0.2}$)	6.6 ± 0.6
V367 Cyg	9.4	$1.3^{+0.2}_{-0.2}$	$2.6^{+0.4}_{-0.4}$	7.3 ± 1.0
W Cru	8.1 (8.7)	$4.0^{+0.9}_{-0.7}$ ($2.3^{+0.5}_{-0.3}$)	$8.0^{+1.8}_{-1.4}$ ($4.6^{+1.0}_{-0.6}$)	9.0
V644 Mon	8.3 (8.6)	$3.3^{+0.7}_{-0.5}$ ($2.5^{+0.6}_{-0.4}$)	$6.6^{+1.4}_{-1.0}$ ($5.0^{+1.2}_{-0.8}$)	...
V1507 Cyg	9.0	$1.8^{+0.3}_{-0.3}$	$3.6^{+0.6}_{-0.6}$...
V356 Sgr	9.0 (9.6)	$1.8^{+0.3}_{-0.3}$ ($1.1^{+0.2}_{-0.1}$)	$3.6^{+0.6}_{-0.6}$ ($2.2^{+0.4}_{-0.2}$)	...

Notes.

^a Log of age in years as measured from nonrotating stellar models. The estimated uncertainties are 0.1–0.2 dex.

^b Mass of star at MSTO obtained from nonrotating stellar models. The quoted errors assume a ± 0.2 dex uncertainty in $\log(t_{\text{yr}})$ (see text).

^c Total system mass assuming an initial mass ratio of unity and conservative mass transfer.

^d Total system mass from Tables 4 and 5 of Mennickent et al. (2016).

V367 Cyg final sample contains a well-defined SGB sequence that follows the isochrone that is consistent with the brightest candidate MSTO star. This suggests that the ages estimated from the isochrones for W Cru, V367 Cyg, V644 Mon, and V1507 Cyg are not skewed by field stars. While the evidence against possible contamination from one or two background stars is not as strong for W Ser and RX Cas, we note that both are near the outer fringes of the main data cloud on the proper motion diagram, reducing the chances of contamination from field stars.

5.2. Estimating Initial Masses

The ages of the groupings and the masses of MSTO stars are listed in the second and third columns of Table 2. The uncertainties in the masses assume a ± 0.2 dex error in $\log(t_{\text{yr}})$ (see previous section). The uncertainties in the MSTO masses do not include systematic errors due to metallicity, reddening, etc. However, errors in these quantities are expected to introduce uncertainties in masses that are smaller than those that arise due to uncertainties in age and in stellar properties, such as the rate of rotation (see below).

If the W Ser systems are experiencing Case B mass transfer, then the donor star was likely on its first transit across the CMD when mass transfer was initiated. As the donor has then only recently evolved off of the main sequence, the *initial* mass of the donor star should not depart markedly from that of a star at the MSTO of the group or cluster in which it is a member (but see caveats below). Given the rapid pace of mass transfer during the initial stages of the interaction (e.g., Nelson & Eggleton 2001), unless the system is viewed at a fortuitous time at the very beginning of mass transfer, the present-day mass of the donor star will be lower than its initial value.

If the mass transfer is a conservative process, then the mass lost from the donor star will remain in the system. Therefore, working under the assumption of conservative mass exchange, if an initial system mass ratio is assumed, then the total system mass can be estimated knowing the initial mass of the donor star. Of course, the present-day mass ratio of these systems is likely very different from the initial value, given that mass transfer is now underway. System mass estimates that assume an initial mass ratio of unity are listed in the fourth column of Table 2. These are upper limits to the system mass, because (1) the donor star must have initially been the more massive star in the system (i.e., the mass ratio must have been less than unity) and (2) the mass transfer process is likely not conservative—at least some mass is almost certainly ejected from the system.

Some of these systems have mass estimates in the published literature. Mennickent et al. (2016) compile mass estimates for the five systems identified by Plavec & Koch (1978), and these masses are listed in the last column of Table 2. These estimates are based on spectroscopic analyses of these systems, and the uncertainties are those listed in Table 5 of Mennickent et al. (2016).

The mass estimates for W Ser systems that are based on photometric and spectroscopic measurements can be highly uncertain, due to assumptions made when interpreting the origins of the signal, as light does not come solely from the component stars. One implication is that absorption and emission features may not track the orbital motions of the components. The range in mass estimates made for a system can be substantial. For example, Davidge (2022a) compiles mass estimates for the components of V367 Cyg, and the various estimates for the total system mass fall between $7 M_{\odot}$ and $33 M_{\odot}$.

Three of the systems do not have mass estimates in the final column of Table 2. We are not aware of modern mass estimates for V1507 Cyg in the published literature. As for V644 Mon and V356 Sgr, Aufdenberg (1994) finds component masses of 4 and $13 M_{\odot}$ for the former, while Fraser et al. (1994) find masses of 3 and $11 M_{\odot}$ for the components of the latter. Details regarding how these masses were determined have not been published, and so we opt not to include them in Table 2. However, if these mass estimates are correct, then V644 Mon and V356 Sgr are the most massive systems in the sample examined here.

With the exceptions of W Ser and W Cru, the initial system masses inferred from the MSTO and assuming a mass ratio of unity are smaller than the masses listed by Mennickent et al. (2016). The MSTO mass estimates in the third column of Table 2 are based on nonrotating stellar models. Rotation-induced mixing delays evolution such that stars with a higher mass will maintain central hydrogen burning longer than nonrotating stars. In fact, a wide dispersion in rotational velocities has been detected in Galactic clusters with ages that are comparable to those of some of the groups found here (e.g., Bastian et al. 2018) and also in intermediate-age clusters in the Large Magellanic Cloud (e.g., Mackey & Broby Neilson 2007). If models that assume $\frac{v}{v_{\text{crit}}} = 0.4$ are used to compute MSTO masses, then the results in the fourth column of Table 2 increase by ~ 0.2 – $0.3 M_{\odot}$ (~ 0.4 – $0.6 M_{\odot}$ for initial system masses), in the sense that higher offsets apply to the youngest systems. This is not sufficient to bridge the gap in masses listed in the fourth and fifth columns of Table 2 for RX Cas, SX Cas, and V367 Cyg. Therefore, while including moderate amounts

of rotation will elevate mass estimates obtained from the MSTO of any cluster/groups, comparatively high rates of rotation among the MSTO stars are required in order to achieve better agreement with the Mennickent et al. (2016) mass estimates.

Of course, another possible (and perhaps more plausible) explanation is that the donor stars in W Ser systems have had their evolution delayed by a mechanism other than rotation. Indeed, as binary systems in which there has been mass transfer, the evolutions of the component stars have likely departed from those expected for single stars that have the same initial masses (e.g., Hurley et al. 2002; Van Rensbergen et al. 2011; Langer 2012; Van Rensbergen & De Greve 2020). We also note that one system, V644 Mon, has been classified as a Be star (Welin 1979, and references therein). Many such objects are rapid rotators, possibly approaching the critical break-up velocity (Townsend et al. 2004).

6. The Circumbinary Environment

Deschamps et al. (2015) model the early stages of mass transfer in CBSs, including mass outflow that is powered by hot spots on the accretion disk that surrounds the secondary star. A circumsystem dust envelope forms as grains condense out of the ejected material, and the resulting envelope may extend out to many au. Deschamps et al. (2015) simulate a system with intermediate-mass components, and they conclude that envelopes around systems at distances out to at least a few hundred parsecs should be observable in the MIR with a moderate-sized space-based telescope. In fact, envelopes like those simulated by Deschamps et al. (2015) are resolved around nearby W Ser stars. Davidge (2022a) examined WISE W2 survey images in order to study the morphology of the envelope around the shell system V367 Cyg. In the present study, W2 images of all eight systems are examined.

The W Ser systems are the brightest sources in these images, and their light profiles swamp faint circumsystem emission. The signal from each system was removed by subtracting out a point-spread function (PSF) that was constructed by median-combining normalized light from isolated stars. Bright and isolated PSF stars were not available in all of the image tiles, and so PSFs were constructed by including stars from many of the fields. This approach has the merit of averaging out structure in the PSF that is a result of the scanning technique used to record the raw images that are ultimately combined to form the final WISE images, coupled with variations in the PSF across the WISE image plane.² The light near the center of the systems has contributions from both the binary system and a fainter envelope, and the PSF was scaled to minimize the residuals near the central regions of each W Ser system in PSF-subtracted images.

PSF-subtracted W2 images are shown in Figure 8. The images in this figure are displayed with a common scaling factor to allow system-to-system variations in envelope brightness to be assessed. Envelopes are detected around W Ser, RX Cas, V367 Cyg, W Cru, and V644 Mon. The prominent central holes indicate that the PSF has been oversubtracted despite having been scaled to minimize residuals. PSF subtraction using a more refined estimate of

the true brightness of the binary system should produce even more prominent envelopes than those seen in Figure 8.

W Cru is the most distant system and so might be expected to have the faintest and most compact envelope when compared with the other systems, if it is in a similar stage of evolution. In fact, the envelope around W Cru is fainter and more compact than those around W Ser, V367 Cyg, and V644 Mon. Factors that are intrinsic to the W Cru system, such as the rate of mass transfer and the properties of the accretion disk hot spot, are also expected to play a role in defining the brightness and spatial extent of a circumsystem envelope.

While not apparent from Figure 8, a weak envelope is also seen around V1507 Cyg. This system is at a distance that is comparable to those that have more prominent envelopes, and so the faint emission in the W2 images is not a distance effect. As for SX Cas and V356 Sgr, there is no convincing evidence for envelopes around these systems. It has been suggested that V356 Sgr is near the end of the rapid mass-transfer phase of evolution (Dominis et al. 2005), and so the dust envelope may be in the process of dissipating. We suspect that V1507 Cyg and SX Cas are also at an evolutionary stage in which a prominent envelope either has not yet formed or is dispersing.

The light distributions in Figure 8 are not azimuthally symmetric, and obvious substructures are seen in the envelopes of all five of the systems in which a disk is evident. The most prominent such structures are in the envelopes around V367 Cyg and V644 Mon. We suspect that these are artifacts of variations in the WISE PSF that are inherent to the raw scans that were combined to make the final images. This can be checked with observations from another facility. However, as demonstrated in Figure 14 of Davidge (2022a), the FWHM of the PSF would have to be in error by almost a factor of two to account for the extended halos that are seen in Figure 8.

7. Comments on Individual Systems

W Ser: The angular and radial distributions of the final and baseline samples of this system do not differ significantly, suggesting that W Ser is not in a recognizable asterism. Nevertheless, there are hints that it belongs to a stellar ensemble that is distinct from most of its neighbors. First, the kinematic properties of the final and baseline samples differ, in the sense that the location of W Ser on the proper motion diagram (Figure 1(a)) is displaced from the majority of its neighbors. The stars in the final sample are thus also displaced on the proper motion plane from the majority of stars in the baseline sample. Second, while the CMD of stars in the final sample is sparsely populated, the sequence defined by final sample stars, which includes a possible SGB star, passes below the $\log(t_{\text{yr}}) = 9.5$ isochrone, which in turn is a few tenths of a dex older than would be inferred for the baseline sample stars. It can be seen from Figure 8 that there are stars that are offset by only a few tens of arcsec (~ 0.1 – 0.2 pc at the distance of W Ser) from the system. If subsequent observations find that these stars are at the same distance as W Ser, then they may have affected the evolution of the system. While it is not clear if these are physically related to W Ser or are foreground/background field stars, stars with a similar intrinsic IR brightness are not seen near the other systems. W Ser is one of only two systems studied here (the other is W Cru) in which the total system mass estimated from the MSTO agrees with a mass estimate based on other means. There is clear evidence for an extended envelope around W Ser in the mid-infrared,

² https://wise2.ipac.caltech.edu/docs/release/allsky/expsup/sec4_4c.html#psf

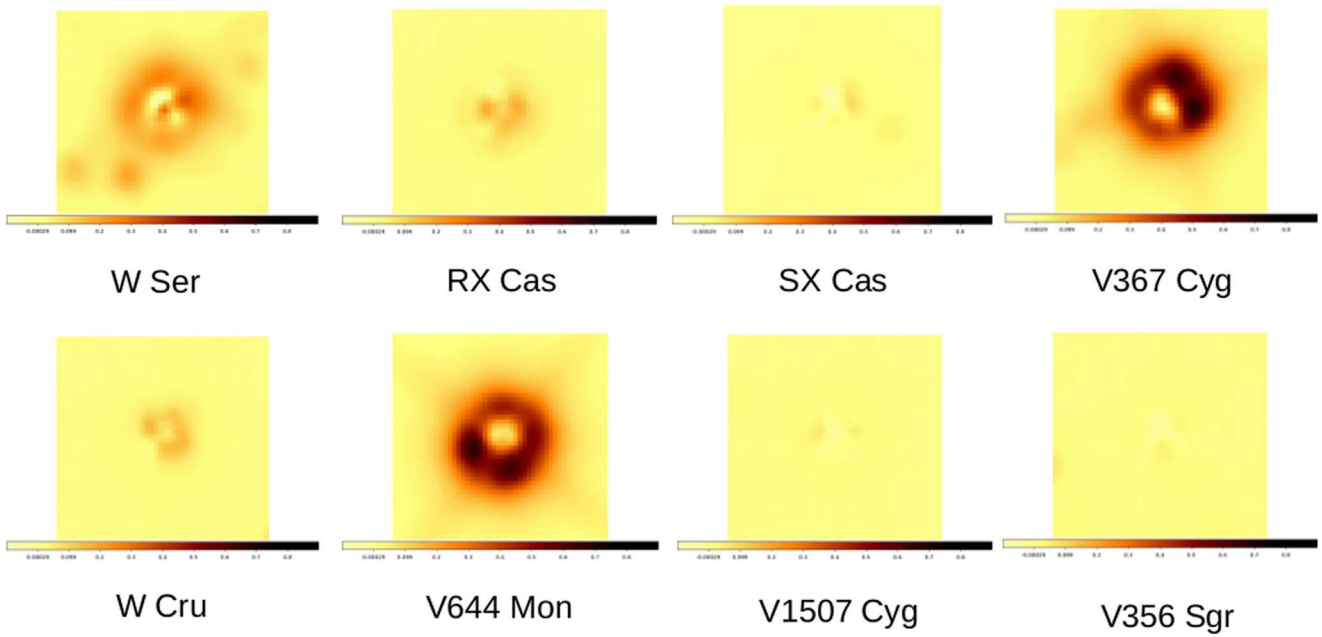


Figure 8. Envelopes around the W Ser systems. Each panel shows an image in W2 that subtends $70'' \times 70''$. A PSF that has been scaled to minimize the residuals near the center of each system has been subtracted from each image, to highlight signal from envelopes and surrounding stars. The PSF-subtracted images are displayed with a common scaling factor to facilitate system-to-system comparisons of envelope brightness. Extended envelopes are clearly seen around W Ser, RX Cas, V367 Cyg, W Cru, and V644 Mon. While not evident in this figure, a very faint envelope is also present around V1507 Cyg. The prominent substructures within the envelopes are likely artifacts of the PSF-subtraction process (see text).

consistent with the notion that it is experiencing rapid mass transfer.

RX Cas: Gaia parallaxes suggest that RX Cas is the closest of the eight systems studied here, and so the final and baseline samples are extracted from the smallest spatial volume. It is then perhaps not surprising that the baseline sample for this system has the smallest number of objects. Like W Ser, the location of RX Cas on the proper motion diagram is offset from the center of the data cloud, indicating that it and the final sample stars have kinematic properties that differ from those of many of its neighbors. Unfortunately, the final sample has only three stars aside from RX Cas itself, and this frustrates efforts to examine the structural properties of the final sample stars and estimate the initial mass of the donor. Still, the angular distribution of final sample stars in Figure 3(a) is lopsided when compared with that of the baseline sample, and this result is significant at the 85% confidence level. While not conclusive, it suggests that, if RX Cas is accompanied by stars that formed with it, then they are now appear to be part of a highly diffuse, stream-like moving group. A search for other members of a moving group associated with RX Cas might then prove to be rewarding. There is evidence for a circumsystem envelope in the W2 images.

SX Cas: SX Cas is unique among the systems studied here, in that the radial distribution of stars in the final sample is more compact than that of stars in the baseline sample, and this is significant at the 95% confidence level. This is consistent with SX Cas being at or near the center of a cluster, lending confidence to the notion that the final sample stars are physically related to SX Cas. The brightest candidate MS star in the final sample is 1.5 mag fainter than the brightest MS star in the baseline sample. There is also a possible SGB star in the final sample, which has the potential to provide leverage for comparisons with isochrones. The CMD of the final sample stars is consistent with $\log(t_{yr}) = 9.4$ or 9.6, depending on the

weight assigned to the SGB star when making comparisons with the isochrones. There is no evidence for an extended envelope in W2, suggesting that SX Cas is in an evolutionary stage that differs from that of most of the other systems. Still, the integrated photometric properties of SX Cas based on the Gaia photometry are very similar to those of W Ser and RX Cas, both of which have extended envelopes.

V367 Cyg: This system is located in a part of the sky where there is active and recent star formation. However, any association with active star-forming regions is likely a projection effect. While V367 Cyg is close to the young cluster M29 on the sky, the parallaxes of the brightest objects in M29 are roughly one half that of V367 Cyg. However, V367 Cyg may be behind some of the dust that obscures this part of the sky. The angular and radial distributions of stars in the baseline and final samples of V367 Cyg are not significantly different, and the angular distributions of both samples are indicative of a lopsided distribution. We suspect that this is due to foreground extinction. The CMD of final sample stars shows a well-defined MSTO complete with an SGB, and the match between the final sample CMD and isochrones is likely the most secure of the systems considered here. The CMD of the final sample stars are matched with a $\log(t_{yr}) = 9.4$ solar-metallicity isochrone, and the corresponding MSTO mass is $1.3M_{\odot}$. Davidge (2022a) reviewed mass estimates for V367 Cyg. Those that include a disk when modeling light curves, and hence presumably have realistic input physics, yield masses of 3.3 and $4.0M_{\odot}$ (Zola & Ogloza 2001), and these were adopted by Mennickent et al. (2016). The reliable comparison with isochrones notwithstanding, the system mass estimated from the MSTO and assuming a mass ratio of unity is much lower than previously published values. As noted by Davidge (2022a), there is a prominent circumsystem envelope visible in the MIR. This may be related to the shell of material that

blankets the system spectrum (e.g., Hack et al. 1984, and references therein).

W Cru: W Cru is the most distant system considered in this paper, and so the final and baseline samples are extracted from a larger volume of space than is the case for the other systems. It is then not surprising that W Cru has the largest baseline sample, and this also means that the final sample is then subject to the highest fractional contamination from field stars. That physically unrelated stellar groupings along the line of sight that have fortuitously similar proper motions might be sampled is of particular concern in richly populated low Galactic latitude fields, such as those in Crux. In fact, the location of W Cru on the proper motion diagram (Figure 1(b)) is near the main concentration of objects in the baseline sample. Still, there is some evidence (albeit marginal) for structural differences between the final and baseline samples, in the sense that the radial distributions of the two samples differ at the 70% confidence level. More significantly, the CMDs of the final and baseline samples clearly differ. The CMD of the baseline sample has a morphology that is reminiscent of the CMDs of field stars (e.g., Babusiaux et al. 2018), and comparisons with solar-metallicity isochrones yield $\log(t_{\text{yr}}) = 9.5$ for stars on the SGB. In contrast, comparisons with isochrones suggest that the stars in the final sample have an age $\log(t_{\text{yr}}) = 8.1$ or 8.7, depending on the weights assigned to the brightest candidate main-sequence star and the possible SGB star that has $G_p \sim 12.5$ and $B_p - R_p \sim 1.4$. If the younger age estimate is adopted, then the total system mass based on the MSTO is close to that found in other studies; in this case, the SGB star is a field interloper. The mass estimates would be in even better agreement if the stars near the MSTO in the final sample CMD evolved with moderate amounts of rotation. The donor star in W Cru has the highest initial mass among the systems considered in this paper, and this is perhaps not surprising, given the long orbital period, the spectral type of the donor star (late-F to early-G supergiant), and the absolute G brightness of the system. The W2 image of W Cru indicates that an envelope is present, so the system is ejecting mass into the surrounding ISM.

V644 Mon: While the projected location of V644 Mon on the sky is close to CMa OB1, the Gaia parallax places it behind this association and related substructures (Santos-Silva et al. 2021). Both the baseline and final samples have lopsided projected on-sky distributions, and we suggest that this is likely due to nonuniform foreground extinction along the line of sight, much of which may be related to CMa OB1. While the V644 Mon final sample is well populated, there is no evidence for structural differences in the angular and radial distributions of stars in the final and baseline samples. Thus, any stellar grouping associated with V644 Mon that contains stars in the current data set does not form an asterism that is distinct from its immediate neighbors. As for the age of V644 Mon, there is a possible SGB star in the final sample, and two ages have been estimated depending on whether or not the red object is matched by the isochrones. Age estimates that differ by 0.3 dex are found, and these produce MSTO mass estimates that differ by $0.4M_{\odot}$. Both estimates predict supersolar initial masses for the donor star, as might be expected given the Be classification (Welin 1979). The donor star in V644 Mon is the second-most massive such object in our sample, and the system has the second-highest absolute G magnitude based on the entries in Table 1. The two systems with the most massive donors

(W Cru and V644 Mon) thus are also the most luminous at visible wavelengths. This is noteworthy because the method used to estimate ages and masses for these systems does not rely on their intrinsic photometric properties, but instead on those of diffusely distributed companion stars. There is evidence for strong, resolved circumsystem emission in the MIR, as might be expected given the Be classification.

V1507 Cyg: The location of V1507 Cyg on the sky places it close to previously identified clusters. It is roughly $50'$ from the moderately young and compact open cluster NGC 6834, although that cluster has a parallax $\pi \sim 0.3$ mas and so is much more distant than V1507 Cyg. Turner 9 is another seemingly nearby cluster, but again it is more distant, with $\pi \sim 0.6$ (Cantat-Gaudin & Anders 2020). Still, there is some evidence for clustering, as the proper motion diagram of the baseline sample shows a concentration of objects with $\mu_{\delta} \sim -4$ mas yr^{-1} and $\mu_{\alpha} \sim -1$ mas yr^{-1} that is offset from V1507 Cyg in this diagram. The majority of the stars in this concentration are not included in the final sample, given the extraction criterion described in Section 3. Nonetheless, there is an obvious lopsided distribution of final sample stars in Figure 3(b), in the sense that the angular distribution of the final sample differs from that of the baseline sample at the 70% confidence level, while the radial distributions of stars in the two samples differ at the 75% confidence level. The former result is consistent with V1507 Cyg being on the periphery of a cluster or moving group. However, the CMD of the baseline sample has a prominent SGB, as expected if there is a large field star population, while there are no candidate SGB stars in the final sample. The MSTO of the final sample, which is close to the brightest main-sequence star in the baseline sample, is consistent with a $\log(t_{\text{yr}}) = 9.0$ solar-metallicity isochrone, which is ~ 0.5 dex younger than the stars on the SGB in the baseline sample. Circumstellar emission is weak in W2 when compared with the other W Ser systems, but it is still present.

V356 Sgr: V356 Sgr is in a crowded field, and neither the angular nor radial distributions of objects on the sky in the final sample differ significantly from that of the baseline sample. There is a ~ 1.5 mag gap between the two brightest MS stars in the final sample, leading to considerable ambiguity in the age estimate. Indeed, depending on the adopted brightness of the MSTO, the CMD is consistent with nonrotating solar-metallicity isochrones having ages $\log(t_{\text{yr}}) = 9$ or 9.6. Despite being one of the closest systems, there is no evidence for extended circumsystem emission. Dominis et al. (2005) suggest that V356 Sgr may be near the end of the rapid mass-transfer phase. If this is the case, then if a circumsystem shell that was comparable to those in the other systems formed earlier, it appears to have dissipated.

8. Discussion and Summary

The classical W Ser systems are interacting binaries that are likely experiencing the rapid phase of mass transfer after the more massive star has evolved to fill its Roche lobe. The masses and ages of the stars in these systems are highly uncertain given the evolved state of one component, which makes it much brighter than its companion, coupled with other sources of light that are not directly related to the components and the presence of an obscuring disk around the gainer. If stars that formed at the same time as these systems can be identified, then it may be possible to estimate their ages and then set limits on the initial mass of the donor star that has (presumably)

recently evolved off of the main sequence. This information is essential to forecast the future evolution of the W Ser systems and place them in the context of CBSs that are in more advanced stages of evolution.

In this study, astrometric and photometric measurements extracted from the Gaia DR3 have been used to identify stars that are associated with five classical W Ser systems and three related objects. A volume with a 10 pc radius on the sky and a depth along the line of sight that depends on the system distance has been searched around each system, to identify possible companions. The 10 pc radius that was adopted for the projected coverage on the sky was selected to sample a moderately diffuse, intermediate-age cluster like the Hyades, and so is a conservative starting point for a search for companions. Meingast et al. (2021) find that the coronae of clusters in the age range 30–300 Myr may extend over distances of 100 pc. However, such coronae are very diffuse, and it is not clear if these would survive over timescales in excess of a Gyr, which we find to be the age for many of the stellar ensembles associated with the W Ser systems. Thus, we prefer to use the more conservative 10 pc search radius.

Two samples of stars have been identified for each W Ser system: one that includes all of the stars within the search volume after filtering based on the uncertainties in the parallax measurements (the baseline sample), and a subset of the baseline sample that has been subject to additional filtering based on proper motions (the final sample). The stars that have distances and kinematic properties that are similar to those of the W Ser systems within this volume are possible fossil remnants of what was once a much larger star cluster. The CMDs of these groupings have been used to estimate ages and initial donor star masses. In some cases, stars in the final sample define an asterism that stands out from the projected distribution of other neighboring stars.

The strengths and morphologies of circumsystem envelopes in the mid-infrared have also been examined using images from the WISE survey. Evidence for extended envelopes is found around most of the systems. System-to-system variation in the strength of this emission is seen, and this is interpreted in the context of differing stages in the evolution of the systems.

8.1. Parallaxes, Proper Motions, and Location on the Sky

Parallaxes are of basic importance for selecting companions of the W Ser systems, and these measurements are likely subject to systematic errors (e.g., Lindegren et al. 2021). While Stassun & Torres (2021) and Ren et al. (2021) describe how these systematics have been reduced in progressive Gaia data releases using eclipsing binaries as calibrators, systematics still remain. In this study, the range of parallaxes that have been searched for companions around each system has been defined to take into account possible systematics that arise due to differences in source brightness. In particular, the range of parallaxes considered for each system is based on the uncertainties in the parallax measurements of that system. This was done because the uncertainties in the parallaxes of the W Ser systems tend to be comparable to the possible systematic errors due to source brightness. Restricting the search volume according to the uncertainty in the parallax thus allows at least some fraction of actual cluster members to be selected even if systematic errors due to source brightness are present.

An unfortunate consequence of the use of the uncertainty in parallax rather than a fixed search depth is that the search

volume increases when systems at progressively larger distance (and hence larger uncertainties in distance) are considered. However, if a fixed physical depth (say 10 pc, corresponding to the projected search radius on the sky) had been employed instead, then the range in parallaxes that are searched would have been smaller than that resulting from the uncertainties in the system parallax, with the result that actual cluster members might be missed if there are systematic errors due to source brightness or if the random uncertainties in parallax are large.

Further mitigation of systematic errors in parallax was provided with other selection criteria. First, the projected area sampled on the sky around each W Ser system is less than a degree in radius, thereby reducing potential systematic errors due to location on the sky. Second, upper limits have been placed on random uncertainties in the parallaxes. This is an obvious criterion to limit the number of sources that physically fall outside the volume of interest but may creep into the sample because of errors in their parallax. It also sets a faint limit in target brightness, thereby reducing systematic uncertainties in parallaxes that might arise due to source brightness.

Proper motions are also critical for the identification of possible companions. Obvious groupings of objects in the proper motion plane are seen around V367 Cyg, W Cru, and V644 Mon. However, similar concentrations are less obvious for the other systems when they are considered individually. An extraction criterion for proper motions was thus found by combining the proper motion diagrams of four of the closest W Ser systems after adjusting for system-to-system differences in proper motion. Clear evidence of clustering in the proper motion plane was found, and the objects in these proper motion groupings are distributed over projected spatial scales on the sky of many parsecs. This indicates a tendency for the W Ser systems to be accompanied by a diffusely distributed group of companions, albeit in small numbers in some cases.

The kinematic properties of systems provide clues into their past evolution, as well as their relationship to other neighboring stars. The baseline sample is expected to contain a diverse mix of stars that spans a range of ages and kinematic properties, and so provides a reference sample for identifying structures that may be present in the final sample. W Ser and RX Cas are offset on the proper motion diagram, in the sense that they are located near the edges of the data distributions defined by the baseline samples. This suggests that the kinematic histories of these systems (as well as any accompanying stars) are distinct from those of the majority of stars in the baseline samples. In contrast, SX Cas, W Cru, and V644 Mon are more-or-less centered on the distribution defined by baseline stars in the proper motion plane.

The projected distribution of stars on the sky in the final and baseline samples provides insights into the environment around the systems. The radial distribution of stars in the final sample of SX Cas differs from that of the baseline sample at the 95% confidence level, and this is consistent with that system being near the center of an organized (but diffuse) asterism. Preliminary (which we interpret as a confidence level between 70% and 95%) evidence is also found for components that have a distribution that is distinct from the baseline samples around RX Cas, W Cru, and V1507 Cyg. In the cases of RX Cas and V1507 Cyg, the distribution of final sample stars on the sky hints that the W Ser system may be near the edge of a cluster or moving group. While there might then be merit to expanding the search area on the sky, we are hesitant to do so with the

existing data, as this increases the risk of contaminants from field stars that have proper motions fortuitously similar to those of the W Ser systems.

Despite efforts to suppress the presence of contaminants using proper motion as a filter, the final samples almost certainly contain sources that are not related to the W Ser systems. The final sample for W Cru is probably the most susceptible to such contamination, as the baseline sample is extracted over a distance of a few hundred pc along the line of sight. However, even in this extreme case, there are hints that contamination from field stars is modest. For example, the distribution of objects on the sky in the baseline and final samples of W Cru differ, albeit at the 70% confidence level. Moreover, the CMD of the W Cru final sample stars differs from that of the baseline population. The reduction of the uncertainties in the parallaxes combined with radial velocity measurements will provide information for confirming the identity of potential cluster members.

8.2. Ages and Masses

The locations of the MSTO in the CMDs of the final samples suggest that only V644 Mon and W Cru have ages that are less than 1 Gyr, although those systems still have ages in excess of 100 Myr. The W Ser systems studied here thus appear to be intermediate-age objects—they are likely not massive, young systems. With the caveat that rotation and tidal effects may impact the pace of stellar evolution, the MSTO mass found from the CMDs of the final samples should be a close approximation to the *initial* mass of the donor star, as that star has presumably recently evolved off of the main sequence. If mass transfer has been more-or-less conservative up to the current epoch, then a total system mass estimate can be made using the masses of MSTO stars in the final samples (column 4 of Table 2) after assuming an initial mass ratio. The total initial system mass calculated in this way is an upper limit, if an initial mass ratio of unity is adopted.

The total initial mass estimates made from the CMDs of the final sample stars are lower than those found from other means (column 5 of Table 2) in three of five cases. What is the cause of the discrepancy between the total mass estimates for RX Cas, SX Cas, and V367 Cyg in Table 2? To begin, mass estimates made from the combined analysis of spectroscopic and photometric information are not free of uncertainties. For example, V367 Cyg, has the best-defined final sample CMD, and so has the greatest potential for achieving a reliable match with isochrones—and hence a reliable MSTO mass. Mass estimates for that system that are based on photometric and spectroscopic observations were reviewed by Davidge (2022a), who found a large range of values, none of which match those in the fourth column of Table 2.

The brightness of the MSTO may have been underestimated in the final samples of RX Cas, SX Cas, and V367 Cyg. This might be expected, given that only a modest number of final sample stars are present, and stochastic effects could then make finding a star at or near the “true” MSTO problematic. With only three stars in the final sample, the total mass estimate for RX Cas is the most vulnerable to stochastic effects. However, the actual MSTO on the CMD would have to be ~ 2 mag brighter than found here to relieve the system mass discrepancy that is evident in Table 2. Even if the brightest blue star in the RX Cas baseline sample were used to estimate the system mass of RX Cas, there would still be a substantial mass discrepancy. As for V367 Cyg,

the final sample CMD of that system is well defined near the MSTO and SGB, and the discrepancy between the donor star mass estimates in Table 2 for this system is typical of those for the other two systems. While we are unable to rule out stochastic effects as a cause of the mass discrepancies for RX Cas and SX Cas, it is unlikely that these can account for all of the differences between the mass estimates of these systems in the fourth and fifth columns of Table 2.

Internal mixing will prolong the lifetime of a star and thereby cause a departure from mass estimates that are made from star models with no internal mixing, such as those applied here to obtain the MSTO masses that in turn serve as proxies for the initial masses of the donor stars. If the donor stars and the MSTO stars have had vastly different internal mixing histories, then this could cause a discrepancy in the total mass estimates. That being said, examining models with moderate amounts of rotation suggest that the change in initial mass with respect to the nonrotating case in the mass range considered here (i.e., just above solar to a few times solar) is at most a few tenths of the M_{\odot} . To produce a large mass discrepancy, the donor stars in the CBSs must have experienced a much greater amount of mixing throughout their lives, prior to the onset of interactions with their companions, than the (presumably) isolated single stars near the MSTO. It would be of interest to obtain spectra of stars near the MSTO in the final samples, to determine if these stars are fast rotators at the present day.

8.3. Circumsystem Emission

If these systems are experiencing rapid mass transfer, then models suggest that there will be a significant outward mass flow, producing circumsystem envelopes. There is well-established spectroscopic evidence for a circumsystem shell around V367 Cyg (Davidge 2022a, and references therein) and other classical W Ser systems (e.g., Broz et al. 2021). Thermal emission will presumably originate in the outermost regions of the shells where grain formation is possible. In Section 7, evidence is presented for resolved envelopes around six of the systems in the MIR. It appears that the strength of the emission in the W2 filter is not correlated with the initial system mass estimates made in Section 5.2. While the most prominent detections are those around V367 Cyg and V644 Mon, these systems have very different initial mass estimates. It is more likely that the MIR emission is related to the rate of mass transfer, as would be consistent with the Deschamps et al. (2015) outflow model. We have spectra of V644 Mon in hand that cover much of its orbital cycle, and in a future paper we will use these to examine the properties of the circumsystem shell and rate of mass transfer.

It is a pleasure to thank the anonymous reviewer for suggestions that greatly improved the manuscript. This research has made use of the NASA/IPAC Infrared Science Archive (<https://doi.org/10.26131/irsa1>), which is funded by the National Aeronautics and Space Administration and operated by the California Institute of Technology. This work has also made use of data from the European Space Agency (ESA) mission Gaia (<https://www.cosmos.esa.int/gaia>), processed by the Gaia Data Processing and Analysis Consortium (DPAC, <https://www.cosmos.esa.int/web/gaia/dpac/consortium>). Funding for the DPAC has been provided by national institutions, in particular the institutions participating in the Gaia Multilateral Agreement.

ORCID iDs

T. J. Davidge  <https://orcid.org/0009-0005-8761-2759>

References

- Aufdenberg, J. P. 1994, AAS Meeting, [185](#), [2110](#)
- Babusiaux, C., van Leeuwen, F., Barstow, M. A., et al. 2018, [A&A](#), [616](#), [A10](#)
- Bastian, N., Kamann, S., Cabrera-Ziri, I., et al. 2018, [MNRAS](#), [480](#), [3739](#)
- Bastian, U. 2019, [A&A](#), [630](#), [L8](#)
- Broz, M., Mourard, D., Budaj, J., et al. 2021, [A&A](#), [645](#), [A51](#)
- Cantat-Gaudin, T., & Anders, F. 2020, [A&A](#), [633](#), [99](#)
- Choi, J., Dotter, A., Conroy, C., et al. 2016, [ApJ](#), [823](#), [102](#)
- Davidge, T. J. 2022a, [AJ](#), [164](#), [149](#)
- Davidge, T. J. 2022b, [RNAAS](#), [6](#), [175](#)
- Davidge, T. J., & Milone, E. F. 1984, [ApJS](#), [55](#), [571](#)
- Deschamps, R., Braun, K., Jurissen, A., et al. 2015, [A&A](#), [577](#), [A55](#)
- Dominis, D., Mimica, P., Pavlovski, K., & Tamajo, E. 2005, [Ap&SS](#), [296](#), [189](#)
- Dotter, A. 2016, [ApJS](#), [222](#), [8](#)
- Fraser, K. L., Roby, S. W., & Polidan, R. S. 1994, *BAAS*, [29](#), [1287](#)
- Gaia Collaboration, Prusti, T., de Bruijne, J. H. J., et al. 2016, [A&A](#), [595](#), [A1](#)
- Gaia Collaboration, Vallenari, A., Brown, A. G. A., et al. 2022, [arXiv:2208.00211](#)
- Hack, M., Engin, S., & Yilmaz, N. 1984, [A&A](#), [131](#), [147](#)
- Halbedel, E. M. 1989, [PASP](#), [101](#), [995](#)
- Hurley, J. R., Tout, C. A., & Pols, O. A. 2002, [MNRAS](#), [329](#), [897](#)
- Jordi, C., Gebran, M., Carrasco, J. M., et al. 2010, [A&A](#), [523](#), [A48](#)
- Langer, N. 2012, [ARA&A](#), [50](#), [107](#)
- Lindegren, L., Bastian, U., Biermann, M., et al. 2021, [A&A](#), [649](#), [A4](#)
- Mackey, A. D., & Broby Neilson, P. 2007, [MNRAS](#), [379](#), [151](#)
- Maeder, A., & Meynet, G. 2000, [ARA&A](#), [38](#), [143](#)
- Meingast, S., Alves, J., & Rottensteiner, A. 2021, [A&A](#), [645](#), [A84](#)
- Mennickent, R. E., Otero, S., & Kolaczowski, Z. 2016, [MNRAS](#), [455](#), [1728](#)
- Muzic, K., Scholz, S., Pena Ramirez, K., et al. 2019, [ApJ](#), [881](#), [79](#)
- Nelson, C. A., & Eggleton, P. P. 2001, [ApJ](#), [552](#), [664](#)
- Paxton, B., Bildsten, L., Dotter, A., et al. 2011, [ApJS](#), [192](#), [3](#)
- Paxton, B., Cantiello, M., Arras, P., et al. 2013, [ApJS](#), [208](#), [4](#)
- Paxton, B., Marchant, P., Schwab, J., et al. 2015, [ApJS](#), [220](#), [15](#)
- Plavec, M., & Koch, R. H. 1978, *IBVS*, [1482](#), [1](#)
- Ren, F., Chen, X., Zhang, H., et al. 2021, [ApJL](#), [911](#), [L20](#)
- Santos-Silva, T., Perottoni, H. D., Almeida-Fernandes, F., et al. 2021, [MNRAS](#), [508](#), [1033](#)
- Song, H. F., Maeder, A., Meynet, G., et al. 2013, [A&A](#), [556](#), [A100](#)
- Stassun, K. G., & Torres, G. 2021, [ApJL](#), [907](#), [L33](#)
- Townsend, R. H. D., Owocki, S. P., & Howarth, I. D. 2004, [MNRAS](#), [350](#), [189](#)
- Van Rensbergen, W., & De Greve, J. P. 2020, [A&A](#), [642](#), [A183](#)
- Van Rensbergen, W., De Greve, J. P., Mennekens, N., Jansen, K., & De Loore, C. 2011, [A&A](#), [528](#), [A16](#)
- Welin, G. 1979, [A&A](#), [79](#), [334](#)
- Wilson, R. E., Rafert, J., & Markworth, N. L. 1984, *IAPPP Comm.*, [16](#), [1](#)
- Wright, E. L., Eisenhart, P. R. M., Mainzer, A. K., et al. 2010, [AJ](#), [140](#), [1868](#)
- Wright, E. L., Eisenhart, P. R. M., Mainzer, A. K., et al. 2019, *AllWISE Source Catalog* (Pasadena, CA: IPAC)
- Zola, S., & Ogloza, W. 2001, [A&A](#), [368](#), [932](#)